Double-spiral magnetic structure of the Fe/Cr multilayer revealed by nuclear resonance reflectivity

M. A. Andreeva,[1,*] R. A. Baulin,[1] A. I. Chumakov,[2,3] R. Rüffer,[2] G. V. Smirnov,[3] Y. A. Babanov,[4] D. I. Devyaterikov,[4] M. A. Milyaev,[4] D. A. Ponomarev,[4] L. N. Romashev,[4] and V. V. Ustinov[4,5]

[1]*Faculty of Physics, M.V. Lomonosov Moscow State University, 119991 Moscow, Russia*
[2]*ESRF-The European Synchrotron, CS 40220, 38043 Grenoble Cedex 9, France*
[3]*National Research Centre "Kurchatov Institute," Pl. Kurchatova 1, 123182 Moscow, Russia*
[4]*M.N. Mikheev Institute of Metal Physics UB RAS, 620990 Ekaterinburg, Russia*
[5]*Institute of Natural Sciences, Ural Federal University, 620083 Ekaterinburg, Russia*

(Received 9 June 2017; published 18 January 2018)

We have studied the magnetization depth profiles in a $[^{57}\mathrm{Fe}(d_{\mathrm{Fe}})/\mathrm{Cr}(d_{\mathrm{Cr}})]_{30}$ multilayer with ultrathin Fe layers and nominal thickness of the chromium spacers $d_{\mathrm{Cr}} \approx 2.0$ nm using nuclear resonance scattering of synchrotron radiation. The presence of a broad pure-magnetic half-order (1/2) Bragg reflection has been detected at zero external field. The joint fit of the reflectivity curves and Mössbauer spectra of reflectivity measured near the critical angle and at the "magnetic" peak reveals that the magnetic structure of the multilayer is formed by two spirals, one in the odd and another one in the even iron layers, with the opposite signs of rotation. The double-spiral structure starts from the surface with the almost-antiferromagnetic alignment of the adjacent Fe layers. The rotation of the two spirals leads to nearly ferromagnetic alignment of the two magnetic subsystems at some depth, where the sudden turn of the magnetic vectors by ∼180° (spin flop) appears, and both spirals start to rotate in opposite directions. The observation of this unusual double-spiral magnetic structure suggests that the unique properties of giant magnetoresistance devices can be further tailored using ultrathin magnetic layers.

DOI: 10.1103/PhysRevB.97.024417

I. INTRODUCTION

Magnetization depth profiles in multilayers consisting of alternating layers of ferromagnetic (FM) and nonmagnetic or antiferromagnetic (AF) materials have attracted nonvanishing interest since 1986, when it was discovered [1] that AF interlayer exchange coupling (IEC) between adjacent Fe layers across a Cr spacer leads to the giant magnetoresistance effect [2,3]. This discovery brought the Nobel Prize to Fert and Grünberg in 2007. There are two widely studied features of the magnetization arrangement between the FM layers. They are (i) the long-period and short-period oscillations of the AF IEC as a function of the thickness of a nonmagnetic spacer [4–7] (more references in the review [8]), and (ii) the intriguing staircase dependence of the hysteresis curves explained by the sequent layer-by-layer rotation of magnetization under the action of the external magnetic field $\mathbf{H}^{\mathrm{ext}}$ [7,9]. The latter observation destroys the simplest picture of the action of the increasing $\mathbf{H}^{\mathrm{ext}}$ on the magnetization alignments in the Fe layers which includes, at first, the rotation to the perpendicular to the $\mathbf{H}^{\mathrm{ext}}$ orientation of the AF coupled Fe layer magnetizations (spin-flop transition) [1,3,10], and afterward the gradual uniform rotation of the two magnetic subsystems to the direction of the external field. In some systems the 90° initial orientation of the two magnetic subsystems have been discovered [11–14], supported by the bilinear-biquadratic formalism or specific proximity magnetism model (Refs. [15,16] and review [8]). However, the theoretical modeling and the more sophisticated experimental techniques, giving the depth-resolved magnetization profiles, like polarized neutron reflectivity (PNR) or nuclear resonance reflectivity (NRR), present a more complicated picture of the depth-resolved magnetization reorientations including the layer-by-layer twisting of the magnetization in each magnetic subsystem [17–27].

For the existence of the AF IEC the spacer thickness should be well matched (e.g., in the [Fe/Cr] case it should be equal to ∼0.9–1.2 nm [2,4]). However, the real value of the spacer thickness in a prepared multilayer differs very often from the nominal parameter due to the technological specificity. Besides, the obtained interface quality and possible impurities essentially influence the IEC (see, e.g., Ref. [28]). One could suggest that if the spacer thickness does not match either AF or FM IEC, the magnetization depth profiles of the [Fe/Cr] system could be as complicated as those observed for AF systems under an application of $\mathbf{H}^{\mathrm{ext}}$. In other words, for the intermediate thickness of the spacer it is plausible to expect complicated magnetization profiles like fan structure, spirals with alternating sign of rotation [29], etc.

Here we present such result for $[^{57}\mathrm{Fe}/\mathrm{Cr}]_{30}$ multilayer with the thickness of Cr spacer intermediate between FM and AF IEC. The two magnetic spirals, relating to the odd and even Fe layers, with different signs of rotation have been revealed. The obtained magnetization profiles have not appeared in the numerous theoretical modeling of the AF superlattices [17,23–25].

II. EXPERIMENTAL DETAILS

The studies were enabled due to the novel Synchrotron Mössbauer Source (SMS) [30,31]. Different from a common

*mandreeva1@yandex.ru

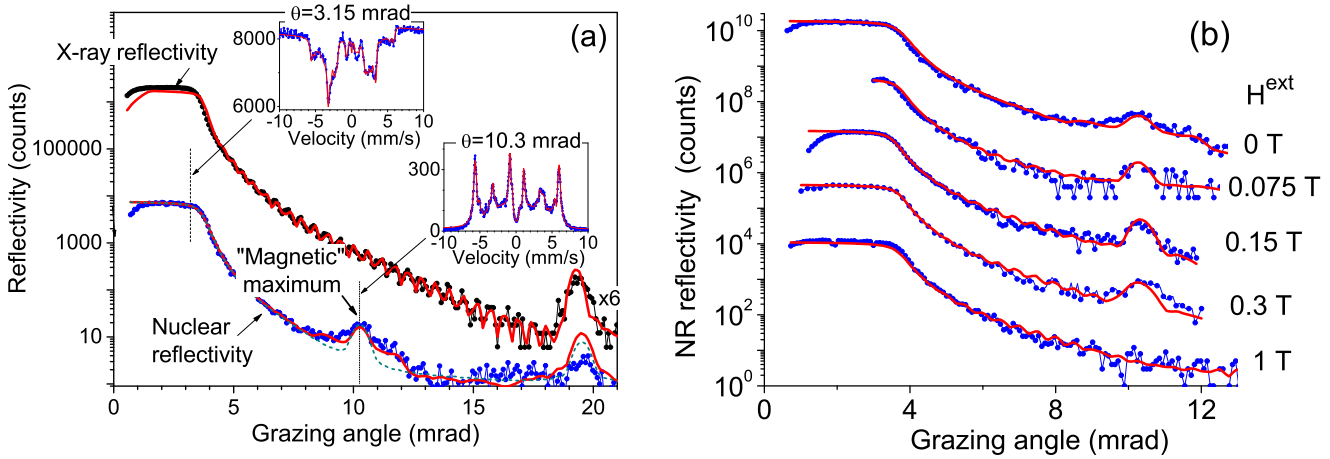

FIG. 1. (a) Electronic and NRR curves measured at 4 K and without $\mathbf{H}^{\text{ext}}$. Insets: Mössbauer spectra of reflectivity, measured near the critical angle of the total reflection and at the magnetic 1/2-order Bragg peak. (b) Evolution of the magnetic 1/2-order peak with $\mathbf{H}^{\text{ext}}$, applied perpendicular to the beam in the surface plane. Symbols are the experimental data, thick (red online) lines are the fit. Thin dashed (green online) line in (a) shows the theoretical spectra for the model of the antiferromagnetic alignments of $\mathbf{B}_{hf}^{(i)}$ giving the 45°/−135° azimuth angles. Curves are shifted vertically for clarity.

radioactive source, the radiation coming from the SMS is the needlelike collimated beam with small (∼mm) size, which can be further focused to spot sizes of few micrometers [31]. It is important that the radiation from SMS is fully π-polarized. These properties make the SMS an ideal device for Mössbauer spectroscopy in the conventional energy scale in reflectivity geometry and supply us the rich information about the magnetization depth profiles in multilayers.

The series of Al_2O_3/Cr(7 nm)/[^{57}Fe(x nm)/Cr(y nm)]$_{30}$/Cr(1.2 nm) samples with ultrathin ^{57}Fe layers (0.08 nm $< x <$ 0.8 nm) and various Cr spacers ($y = 1.05$, 2.0 nm) was grown at the Katun'-C molecular-beam epitaxy facility in the Institute of Metal Physics in Ekaterinburg, Russia.

The measurements were performed at the Nuclear Resonance beamline [32] ID18 of the European Synchrotron Radiation Facility (ESRF). The storage ring was operated in multibunch mode with a nominal storage ring current of 200 mA. The energy bandwidth of radiation was first reduced down to 2.1 eV by the high-heat-load monochromator [33], adjusted to 14.4125 keV energy of the nuclear resonance transition in the ^{57}Fe. Then x rays were collimated by the compound refractive lenses down to the angular divergence of a few μrad. The high-resolution monochromator decreases the energy bandwidth of the beam further to ∼15 meV. Final monochromatization down to the energy bandwidth of ∼8 neV was achieved using the SMS [30,31]. Radiation from the SMS was focused down to the beam size of $8 \times 10\,\mu\text{m}^2$ using the Kirkpatrick-Baez multilayer mirror system. The intensity of the beam on the sample site was $\sim 10^4$ photons/s.

The scan through the resonant spectrum in the energy range of about $\pm 0.5\,\mu$eV was executed using the method of the Doppler shift, common in Mössbauer spectroscopy, i.e., by vibrating the SMS along the beam direction. NRR curves have been obtained by integration over the Mössbauer spectra of reflectivity at each incidence angle. X-ray reflectivity has been measured using the Renninger reflection option of the SMS [31], where SMS provides radiation in the energy bandwidth of ∼15 meV.

For varying temperature and $\mathbf{H}^{\text{ext}}$, the samples were mounted in the cassette holder and placed into the He-exchange gas superconducting cryomagnetic system. The experimental data were analyzed with our program package REFSPC, developed specifically for these studies and uploaded to the ESRF scientific software website [34].

The results for the samples with ultrathin ^{57}Fe layers (∼0.1–0.2 nm) which did not show any periodicity either in the electronic or in the NR reflectivity were presented in Ref. [35]. The [^{57}Fe(0.8 nm)/Cr(1.05 nm)]$_{30}$ sample (the nominal thicknesses are pointed out) demonstrated the expected typical AF interlayer coupling, and peculiarities of the measured spectra were discussed in Ref. [36]. Here we present the result for the [^{57}Fe(0.8 nm)/Cr(2.0 nm)]$_{30}$ sample for which we have supposed a pure FM ordering between ^{57}Fe layers, but have discovered the very complicated magnetization profile.

III. DATA TREATMENT

Figure 1 shows the electronic and NRR curves for the Al_2O_3/Cr(7 nm)/[^{57}Fe(0.8 nm)/Cr(2.0 nm)]$_{30}$/Cr(1.2 nm) sample. The measurements were performed at 4 K. The fit of the electronic reflectivity curve gives the period of the structure of 2.24 nm with 1.58 nm for the Cr layer thickness, which corresponds in reality to the intermediate value between FM and AF IEC.

The depth profile of the electronic density is presented in Fig. 2. It is used and kept unchanged in the fit of the NRR curves and Mössbauer spectra of reflectivity. Taking into account the different orientations of the hyperfine fields $\mathbf{B}_{hf}^{(i)}$, in subsequent ^{57}Fe layers the model includes 64 layers; the interface are presented by the additional steps approximating the error function.

The NRR curve surprisingly shows a small bump at the position corresponding to the half-order (1/2) Bragg peak. The smeared maximum at ∼10 mrad in the NRR curve has a pure magnetic origin. This is confirmed by the external field $\mathbf{H}^{\text{ext}}$ application. Figure 1(b) shows that applying $\mathbf{H}^{\text{ext}}$

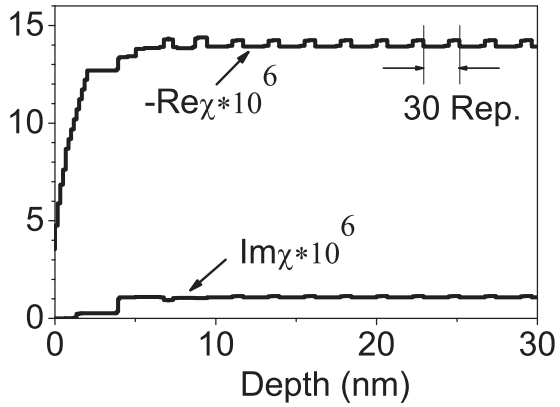

FIG. 2. Depth dependence of the real and imaginary parts of the electronic susceptibility $\chi^{el} = 2(n-1)$ (n is a refraction index) for our sample obtained by the fit of the electronic reflectivity curve.

firstly increases the "magnetic" peak, and then suppresses it. The presence of the half-order magnetic maximum could be interpreted by the doubling of the chemical period due to the AF ordering between ^{57}Fe layers. However, this magnetic maximum has a rather smeared shape, and in addition an unusual distortion of the first-order Bragg peak is seen in the NRR curve. Such a satellitelike distortion of the peaks evidences the more complicated than AF ordering of the ^{57}Fe layer magnetization. Indeed, the model calculations for various kinds of noncollinear magnetic ordering [37] show that, in order to have the existence of the magnetic maximum and simultaneously the satellites near the first-order Bragg peak, the magnetic structure of the multilayer should include partially spiral and partially AF alignments of the magnetic moments of iron layers.

For the interpretation of the peculiarities of the NRR curves, the Mössbauer spectra of reflectivity can give the additional information. The Mössbauer spectra of reflectivity were measured at the two angles of incidence (Fig. 3): near the critical angle and at the magnetic peak. The obtained distribution of the hyperfine field values $|\mathbf{B}_{hf}^{(i)}|$ is rather complicated (Fig. 4). That is typical for the ultrathin ^{57}Fe layers with interfaces compared with the layer thickness and the ^{57}Fe nuclei have various nearest-neighbor surroundings. It is reasonable to start the fit of the spectra from the case when the hyperfine fields are already completely aligned by the external field [as we see from Fig. 1(b) it happens at ~1 T]; however, at this $\mathbf{H}^{ext}$ the magnetic maximum disappears so we have only the spectrum measured near the critical angle [Fig. 3(b)]. Besides, with π-polarized incident radiation from SMS the alignment of the $\mathbf{B}_{hf}$ in the direction perpendicular to the beam leaves only the second and fifth lines (with the change of the magnetic quantum numbers $\Delta m = 0$) in the Mössbauer spectra of reflectivity, which are poorly resolved. It is difficult to get the depth distribution of the hyperfine fields across the repetition period with only one spectrum of reflectivity. On the other hand, for the spectra measured at a weaker or zero $\mathbf{H}^{ext}$ the depth distribution of the azimuth angles for $\mathbf{B}_{hf}$ in addition to the depth distribution of the $\mathbf{B}_{hf}^{(i)}$ values should be taken into account. So, the fit requires some kind of iteration between data, obtained with different magnitudes of $\mathbf{H}^{ext}$. For each value of $\mathbf{H}^{ext}$ the joint fit of the model NRR curves and available Mössbauer spectra of reflectivity to the experimental ones has been applied.

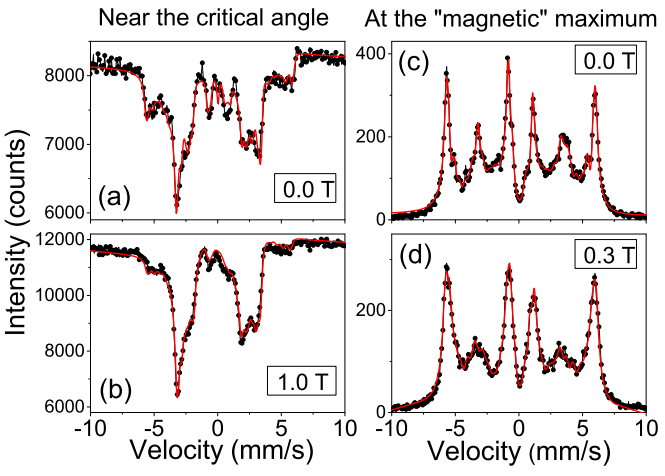

FIG. 3. Mössbauer spectra of reflectivity, measured near the critical angle (at ~3.15 mrad) and at the magnetic 1/2-order peak (at ~10.3 mrad) for various $\mathbf{H}^{ext}$, applied perpendicular to the beam direction in the surface plane. Symbols are the experimental data, thick (red online) lines are the best-fit result. The velocity scale is relative to the Mössbauer spectrum of α iron.

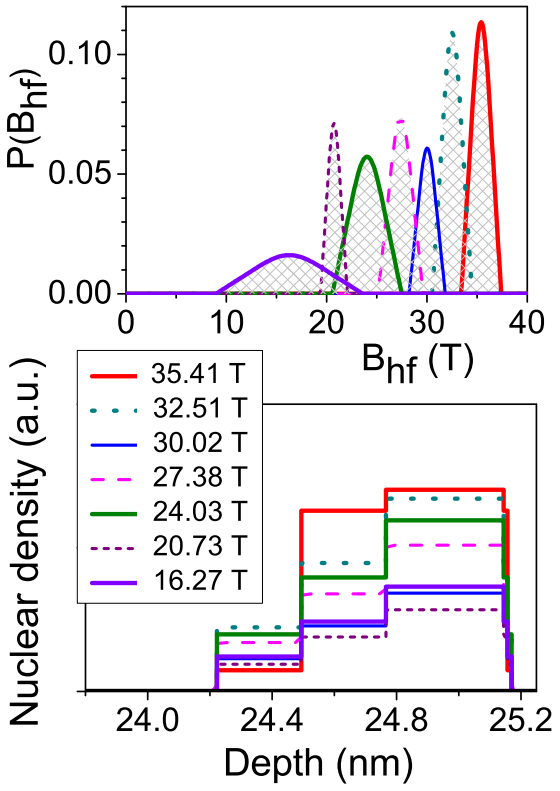

FIG. 4. Top graph: Hyperfine field distribution $P(B_{hf}^{(i)})$, described by seven broad sextets ($i = 1,...7$), obtained by the fit of the theoretical spectra and NRR curves to the experimental ones in Figs. 1, 3. Bottom graph: The obtained depth distribution of these hyperfine fields in one repetition period. Notice that the Cr-on-Fe interfaces are much broader than Fe-on-Cr interfaces. This is in agreement with the results of Ref. [38].

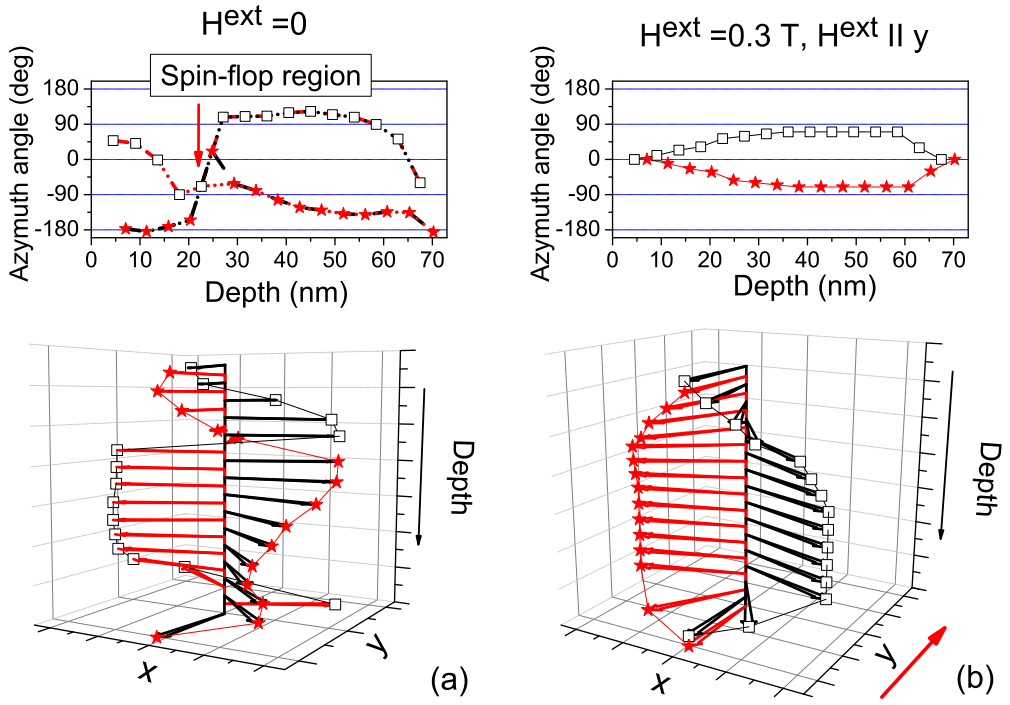

FIG. 5. Depth profile of the orientation of the hyperfine magnetic fields in iron layers without $\mathbf{H}^{\text{ext}}$ (a) and with $\mathbf{H}^{\text{ext}} = 0.3\,\text{T}$, applied along the y axis (b). The asterisks mark even iron layers, whereas squares mark odd iron layers.

The comparison of Figs. 3(c) and 3(d) shows that the intensity of the second and fifth lines of the spectra, corresponding to the $\Delta m = 0$ hyperfine nuclear transitions (located at $\sim\pm 3\,\text{mm/s}$), are noticeably higher at $\mathbf{H}^{\text{ext}} = 0$ than at $\mathbf{H}^{\text{ext}} = 0.3\,\text{T}$. In the case of the symmetric relative to the beam direction alignment of the magnetic moments in the adjacent iron layers, these lines should be entirely suppressed in the Mössbauer spectra at the magnetic peak [36]. Thus, their appearance in the measured spectra evidences the noncollinear and asymmetrical alignment of magnetizations in the adjacent ^{57}Fe layers.

After hyperfine field matching, the depth variation of the azimuth angles for $\mathbf{B}_{hf}$ in ^{57}Fe layers has been performed during the joint fit of the NRR curve and Mössbauer spectra of reflectivity measured in the absence of $\mathbf{H}^{\text{ext}}$. We supposed that azimuth angle is the same for all $\mathbf{B}_{hf}^{(i)}$ in each ^{57}Fe layer, otherwise the number of variables would be too large. It reveals a rather unusual [Fig. 5(a)] depth dependence of $\mathbf{B}_{hf}$ orientations. The magnetic structure forms two spirals, one for the odd and another one for the even iron layers, with the opposite signs of rotation, i.e., with opposite chirality. This double-spiral structure starts near the top of the surface from the almost-AF alignment of the adjacent Fe layers. The rotation of two spirals in the opposite directions leads to the nearly FM alignment of the magnetic moments in the odd and even iron layers at some depth. Here the sudden turn of the magnetic moments in each magnetic sublattice by $\sim 180^\circ$ happens (the spin-flop effect). At larger depths, both spirals change the direction of rotation, still keeping the opposite sign of chirality.

In order to demonstrate the sensitivity of the method to the $\mathbf{B}_{hf}$ orientations, we compare the theoretical Mössbauer spectra of reflectivity calculated for that presented in Fig. 5(a) model and for the model with the AF alignments of $\mathbf{B}_{hf}$, giving the best-fit $45°/-135°$ azimuth angles (Fig. 6). The same comparison is shown in Fig. 1(a) for the NRR curve. It is seen that the simple AF alignments of $\mathbf{B}_{hf}$ give the theoretical NRR curve without satellitelike broadening of the 1/2- and first-order Bragg peaks. Probably that is the most clear proof of the complicated magnetization profile in our sample in the absence of $\mathbf{H}^{\text{ext}}$.

Ramping $\mathbf{H}^{\text{ext}}$ to 0.075 and 0.15 T leads to the noticeable increase of the magnetic Bragg peak [Fig. 1(b)]. Here the fit gives a simple picture of the pure AF alignment of the

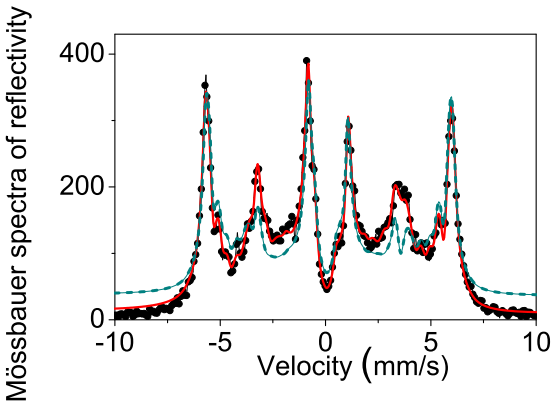

FIG. 6. Mössbauer spectra of reflectivity, measured at the magnetic maximum. The thick (red online) lines are the fit result with the obtained model of the $\mathbf{B}_{hf}$ orientations presented in Fig. 5(a). Thin dashed (green online) line shows the theoretical spectra of the best fit with the model of the AF alignments of $\mathbf{B}_{hf}$ giving the $45°/-135°$ azimuth angles for $\mathbf{B}_{hf}$ orientations.

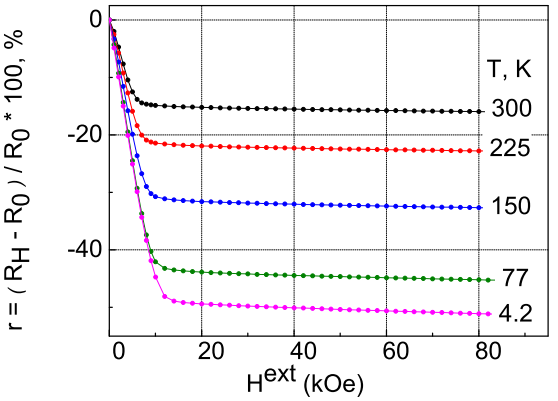

FIG. 7. Magnetic resistivity of the Al_2O_3/Cr(7 nm)/$[^{57}Fe(0.8\,nm)/Cr(2.0\,nm)]_{30}$/Cr(1.2 nm) sample as a function of the applied field at various temperatures.

magnetic vectors perpendicular to the direction of $\mathbf{H}^{ext}$. At stronger $\mathbf{H}^{ext} = 0.3$ T, the $\mathbf{B}_{hf}$ on the ^{57}Fe nuclei begins to align antiparallel to $\mathbf{H}^{ext}$ (that means that the magnetization of ^{57}Fe begins to align parallel to $\mathbf{H}^{ext}$), but not jointly; this rotation starts from the top and bottom layers, where IEC is smaller [Fig. 5(b)]. This picture is in agreement with the theoretical consideration in, e.g., Refs. [23,39].

Note that the direction of the hyperfine magnetic fields $\mathbf{B}_{hf}^{(i)}$ is opposite to the direction of iron magnetic moments and layer magnetization (which is well known since 1964 [40]; some recent measurements in high external field are described in Ref. [41]). Therefore, the antiparallel alignment of the hyperfine fields relative to $\mathbf{H}^{ext}$ means the alignment of the Fe layer magnetization along $\mathbf{H}^{ext}$.

For yet stronger (but still relatively small) $\mathbf{H}^{ext} \approx 1.0$ T, the iron layer magnetizations set in pure FM alignment and the magnetic peak disappear [Fig. 1(b)]. Note that due to the antiparallel alignment of the $\mathbf{B}_{hf}$ and $\mathbf{H}^{ext}$ the hyperfine splitting of the Mössbauer spectra of reflectivity becomes smaller because the nuclei "feel" the total field ($\mathbf{B}_{hf}^{(i)} + \mathbf{H}^{ext}$). This effect has been taken into account during the fit. The magnetic resistivity measurements as well confirm the stabilization of the structure in ferromagnetic state at $\mathbf{H}^{ext} \approx 1.0$ T (Fig. 7).

The double-spiral magnetic structure with the opposite signs of rotations for two spirals and the alteration of the rotation direction with depth [Fig. 5(a)] is our main observation. Analyzing the possible origin of this phenomenon, we note that the magnetization spin flop most often appears for systems with an essentially large plane anisotropy and under an applied magnetic field [17,23]. The Fe/Cr system studied here is characterized by the almost-negligible plane anisotropy. This most probably rules out this reason from possible explanations. The studied system is specific in the ultrasmall thickness of the magnetic Fe layer and in the thickness of the Cr spacer, which is intermediate for FM and AF exchange coupling. Therefore, the observed unique noncollinear double-spiral alignment of the AF lattices is possibly promoted by the attenuation of the IEC between the adjacent iron layers due to a rather thick spacing. This makes the interaction between the next neighbors (long-range interaction) more important, and initiates the observed swirling magnetic ordering.

IV. CONCLUSIONS

In summary, we studied the magnetic structure of the $[Fe/Cr]_{30}$ multilayer with the ultrafine thickness of Fe layers of ~0.66 nm and the thickness of the Cr spacer of 1.58 nm, which is an intermediate between the thicknesses optimal for FM or AF IEC. The obtained magnetization depth profile in iron layers shows up as a double-spiral structure, where the spiral of the odd Fe layers is opposite in chirality to the spiral of the even layers. The result suggests that the unique properties of giant magnetoresistance devices can be further tailored using ultrathin magnetic layers.

From the methodological point of view, we have demonstrated that the NRR method on the basis of the SMS provides us with the exceedingly rich information which gives the opportunity for the more or less correct determination of the magnetic structure. It takes place because the measurements of the reflectivity curves—-both with electronic and nuclear resonance scattering—-is accompanied by the measurements of the Mössbauer spectra of reflectivity for several incidence angles. The unique depth sensitivity of the Mössbauer reflectivity spectra, measured at different grazing angles, provides the distinct advantage of nuclear resonance reflectivity in comparison to other techniques, e.g., to the PNR.

ACKNOWLEDGMENTS

The research was carried out within the state assignment of Russian Federal Agency for Scientific Organizations on the theme "Spin" No. 01201463330 and the Project No. 1.1.3.5. of the Program No. 32 of the Presidium of Russian Academy of Sciences and it was supported in part by the Russian Foundation for Basic Research (Grants No. 15-02-01674-a, No. 15-02-01502-a, No. 16-02-00061-a, and No. 17-02-00142-a).

[1] P. Grünberg, R. Schreiber, Y. Pang, M. B. Brodsky, and H. Sowers, Phys. Rev. Lett. **57**, 2442 (1986).

[2] M. N. Baibich, J. M. Broto, A. Fert, F. Nguyen Van Dau, F. Petroff, P. Etienne, G. Creuzet, A. Friederich, and J. Chazelas, Phys. Rev. Lett. **61**, 2472 (1988).

[3] G. Binasch, P. Grünberg, F. Saurenbach, and W. Zinn, Phys. Rev. B **39**, 4828 (1989).

[4] S. S. P. Parkin, N. More, and K. P. Roche, Phys. Rev. Lett. **64**, 2304 (1990).

[5] S. Demokritov, J. A. Wolf, and P. Grünberg, Europhys. Lett. **15**, 881 (1991).

[6] L. Lazar, J. S. Jiang, G. P. Felcher, A. Inomata, and S. D. Bader, J. Magn. Magn. Mater. **223**, 299 (2001).

[7] S. T. Purcell, W. Folkerts, M. T. Johnson, N. W. E. McGee, K. Jager, J. aan de Stegge, W. B. Zeper, W. Hoving, and P. Grünberg, Phys. Rev. Lett. **67**, 903 (1991).

[8] B. Heinrich and J. F. Cochran, Adv. Phys. **42**, 523 (1993).

[9] V. V. Ustinov, M. A. Milayev, L. N. Romashev, T. P. Krinitsina, A. M. Burkhanov, V. V. Lauter-Pasyuk, and H. J. Lauter, J. Magn. Magn. Mater. **300**, e281 (2006).
[10] K. Temst, E. Kunnen, V. V. Moshchalkov, H. Maletta, H. Fritzsche, and Y. Bruynseraede, Physica B **276–278**, 684 (2000).
[11] P. Grünberg, S. Demokritov, A. Fuss, R. Schreiber, J. A. Wolf, and S. T. Purcell. J. Magn. Magn. Mater. **104–107**, 1734 (1992).
[12] A. Schreyer, J. F. Ankner, Th. Zeidler, H. Zabel, C. F. Majkrzak, M. Schäfer, and P. Grünberg, Europhys. Lett. **32**, 595 (1995).
[13] A. Schreyer, J. F. Ankner, Th. Zeidler, H. Zabel, M. Schäfer, J. A. Wolf, P. Grünberg, and C. F. Majkrzak, Phys. Rev. B **52**, 16066 (1995).
[14] T. Diederich, S. Couet, and R. Röhlsberger, Phys. Rev. B **76**, 054401 (2007).
[15] J. C. Slonczewski, J. Appl. Phys. **73**, 5957 (1993).
[16] J. C. Slonczewski, J. Magn. Magn. Mater. **150**, 13 (1995).
[17] R. W. Wang, D. L. Mills, E. E. Fullerton, J. E. Mattson, and S. D. Bader, Phys. Rev. Lett. **72**, 920 (1994).
[18] V. V. Ustinov, N. G. Bebenin, L. N. Romashev, V. I. Minin, M. A. Milyaev, A. R. Del, and A. V. Semerikov, Phys. Rev. B, **54**, 15958 (1996).
[19] S. Rakhmanova, D. L. Mills, and E. E. Fullerton, Phys. Rev. B **57**, 476 (1998).
[20] S. G. E. te Velthuis, J. S. Jiang, S. D. Bader, and G. P. Felcher, Phys. Rev. Lett. **89**, 127203 (2002).
[21] V. Lauter-Pasyuk, H. J. Lauter, B. P. Toperverg, L. Romashev, and V. V. Ustinov, Phys. Rev. Lett. **89**, 167203 (2002).
[22] C. L'abbé, J. Meersschaut, W. Sturhahn, J. S. Jiang, T. S. Toellner, E. E. Alp, and S. D. Bader, Phys. Rev. Lett. **93**, 037201 (2004).
[23] J. Meersschaut, C. L'abbé, F. M. Almeida, J. S. Jiang, J. Pearson, U. Welp, M. Gierlings, H. Maletta, and S. D. Bader, Phys. Rev. B **73**, 144428 (2006).
[24] V. V. Ustinov, J. Magn. Magn. Mater. **310**, 2219 (2007).
[25] A. I. Morosov and A. S. Sigov, Usp. Fiz. Nauk **180**, 709 (2010).
[26] M. Andreeva, A. Gupta, G. Sharma, S. Kamali, K. Okada, and Y. Yoda, Phys. Rev. B **92**, 134403 (2015).
[27] K. Schlage, R. Röhlsberger, T. Klein, E. Burkel, C. Strohm, and R. Rüffer, New J. Phys. **11**, 013043 (2009).
[28] S. Honda, H. Yanagihara, J.-I. Inoue, E. Kita, H. Itoh, and K. Mibu, Phys. Procedia **75**, 1080 (2015).
[29] R. E. Camley, J. Kwo, M. Hong, and C. L. Chien, Phys. Rev. Lett. **64**, 2703 (1990).
[30] G. V Smirnov, U. van Bürck, A. I. Chumakov, A. Q. R. Baron, and R. Rüffer, Phys. Rev. B **55**, 5811 (1997).
[31] V. Potapkin, A. I. Chumakov, G. V. Smirnov, J.-P. Celse, R. Rüffer, C. McCammon, and L. Dubrovinsky, J. Synchrotron Radiat. **19**, 559 (2012).
[32] R. Rüffer and A. I. Chumakov, Hyperfine Interact. **97/98**, 589 (1996).
[33] A. I. Chumakov, I. Sergeev, J.-Ph. Celse, R. Rüffer, M. Lesourd, L. Zhang, and M. Sanchez del Rio, J. Synchrotron Radiat. **21**, 315 (2014).
[34] http://www.esrf.eu/computing/scientific/REFTIM/MAIN.htm.
[35] M. A. Andreeva, R. A. Baulin, A. I. Chumakov, R. Rüffer, G. V. Smirnov, Y. A. Babanov, D. I. Devyaterikov, B. Yu. Goloborodsky, D. A. Ponomarev, L. N. Romashev, and V. V. Ustinov, J. Met., Mater. Miner. **440**, 225 (2017).
[36] M. A. Andreeva, R. A. Baulin, A. I. Chumakov, R. Rüffer, G. V. Smirnov, Yu. A. Babanov, D. I. Devyaterikov, M. A. Milyaev, D. A. Ponomarev, L. N. Romashev, and V. V. Ustinov, J. Synchrotron Radiat. (to be published).
[37] R. A. Baulin and M. A. Andreeva, Moscow Univ. Phys. Bull. **71**, 180 (2016).
[38] N. V. Bagrets, E. A. Kravtsov, M. A. Milyaev, L. N. Romashev, A. V. Semerikov, and V. V. Ustinov, The Physics of Metals and Metallography **96**, 80 (2003) [Fizika Metallov i Metallovedenie **96**, 88 (2003)].
[39] A. I. Morosov and A. S. Sigov, Phys. Usp. **53**, 677 (2010).
[40] N. Blum and L. Grodzins, Phys. Rev. **136**, A133 (1964).
[41] C. Strohm, P. Van der Linden, and R. Rüffer, Phys. Rev. Lett. **104**, 087601 (2010).